Journal of Energy Challenges and Mechanics
http://www.nscj.co.uk/JECM/

ISSN 2056-9386
Volume 3 (2016) issue 3, article 5

Energy Harvesting Circuit for Radio Frequency Application

无线电频率应用之能量收集电路

Haruichi Kanaya

Department of Electronics, Graduate School of Information Science and Electrical Engineering, Kyushu University, Fukuoka 819-0395, Japan

kanaya@ed.kyushu-u.ac.jp

Accepted for publication on 3rd September 2016

Abstract - **Battery-free or autonomous wearable electronics have attracted great interest in both information communication and medical research. Energy harvesting systems for the radio frequency (RF) region feature long-range energy transmission. However, because the RF receiving signal is so weak, the conversion efficiency is low. In this study, to enhance the amplitude of the RF receiving signal, a resonant circuit is constructed in front of the boosting circuit. The impedance matching circuit, the resonant circuit, and the Cockcroft–Walton (CW) circuit are connected to each other. Moreover, the proposed circuit is mounted on the backside of a one-sided directional antenna on a flexible substrate. This antenna is composed of a coplanar waveguide and a slot on the top metal surface and the bottom floating metal layer. The simulated output DC voltage is 2.89 V for an input of 100 mV and a 50-Ω power source at 900 MHz, and the power efficiency is 58.7% for a 10-MΩ load resistance. In our design method, it is easy to increase the output voltage by optimizing the element number of the CW circuit and the quality factor of the LC resonant circuit.**

Keywords - **Energy harvesting circuit, impedance matching circuit, booster circuit, flexible antenna, one-sided directional antenna.**

I. INTRODUCTION

Recently, battery-free or autonomous wearable electronics have attracted great interest in medical, infrastructure and factory monitoring, and information communication devices [1]–[4]. Radio frequency (RF) energy harvesting systems are suitable for long-range or indoor operation.

Radio frequency identification (RFID) systems in the UHF (ultrahigh frequency) band have become very popular in various applications, such as distribution logistics and human tracking. UHF band RFID systems have long-range identification ability and high-speed data rate compared to other frequency regions. However, they have a disadvantage in their limited amount of RF power and low conversion efficiency.

A number of booster circuits have been reported for a radio frequency identification (RFID) system [5]–[7]. The Cockcroft–Walton circuit (CW circuit) [8] and the modified CW circuit are composed of diode and capacitor pairs and are easy to implement as on-board circuits. In the RF region, there are a number of parasitic elements in the diode and capacitor that degrade the RF boosting properties. Moreover, the RF receiving signal is so weak that an enhancement circuit, such as an LC resonance circuit, and an impedance matching circuit are needed in the RF region.

If an omnidirectional antenna such as a slot antenna that receives RF signals is mounted on a metallic object surface or non-planar object surface such as a can or bottle, its radiation properties are remarkably deteriorated because of electro-magnetic interference. There are several reports about tag antennas such as patch- or label-type antennas for metallic object applications [9–12]. Kanaya et al. [13–15] presented the design method of a one-sided directional slot antenna for IMS band (@2.4 GHz) applications, with an attached floating metal layer on the bottom side and optimized length of the metal layer. An impedance matching circuit is also realized by using an interdigital gap and conductor-backed coplanar waveguide (CPW) transmission line [16, 17]. Based on this design theory, a one-sided directional slot antenna for 900-MHz band RFID systems has been reported on a flexible substrate [18].

In the present study, a resonant circuit was constructed in front of the booster circuit to enhance the amplitude of the RF signal. Moreover, this harvesting circuit was mounted on the backside of a one-sided directional slot antenna. The proposed antenna was designed with the aid of a commercial three-dimensional electromagnetic field simulator (Ansoft; HFSS).

The antenna was fabricated and measured to verify the RF properties. We also successfully lit an LED without connecting it to the power source using wires. This paper is organized as follows. Section II describes the booster circuit design. Section III shows the design method of the impedance matching circuit. Section IV describes the antenna design. The implementation and measurement results are provided in Section V and Section VI. Finally, the conclusion is presented in Section VII.

II. Circuit Design

Figure 1 shows a block diagram of the proposed energy harvesting circuit with a one-sided directional flexible antenna. The antenna, the impedance matching circuit, the resonant circuit, and the CW circuit are connected to each other. The resonant circuit can enhance the RF signal. The individual circuit blocks are described in more detail in the following paragraphs.

Figure 2 shows the unit cell of the CW circuit. The CW circuit comprises two pairs of capacitors and diodes. When the input voltage reaches its negative peak, current flows through the diode charge the left side of the capacitor to an input voltage. When the input voltage reverses polarity and reaches its positive peak, it is added to the left side capacitor's voltage, and the right side capacitor is charged to the double of the input voltage [8].

The output voltage of the CW circuit (V_{out}) is represented theoretically as follows:

$$V_{\text{out}} = V_{\text{in}} \times 2N \tag{1}$$

where V_{in} represents the input voltage, N is the number of capacitors and the diode unit structure, and V_{out} is multiplied by $2N$.

$$| I_S | = \frac{E}{\sqrt{R_S^{\,2} + (X_{LS} - X_{CS})^2}} \tag{2}$$

where X_{LS} and X_{CS} represent ωL_S and $1/\omega C_S$, respectively.

At the resonance condition, resonance current I_0 is given by

$$I_0 = E / R_S \tag{3}$$

In this case, the normalized voltage of L_S or C_S is described as

$$\frac{E_L}{E} = \frac{E}{R_S} X_{LS} \cdot \frac{1}{E} = \frac{X_{LS}}{R_S} \tag{4}$$

and

$$\frac{E_C}{E} = \frac{E}{R_s} X_{CS} \cdot \frac{1}{E} = \frac{X_{CS}}{R_S} \tag{5}$$

Thus, the quality factor of this circuit (Q_S) is given by

$$Q_S = \frac{X_{LS}}{R_S} = \frac{X_{CS}}{R_S} \tag{6}$$

We can obtain the output voltages E_L and E_C, which are Q_S times larger than E. In our energy harvesting circuit, the input RF voltage signal is enhanced by using the above *LCR* series resonance circuit.

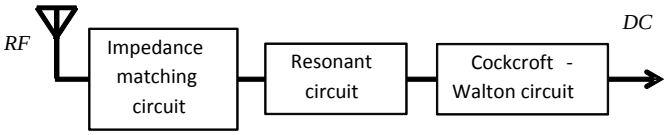

Fig.1. Block diagram of the proposed booster circuit.

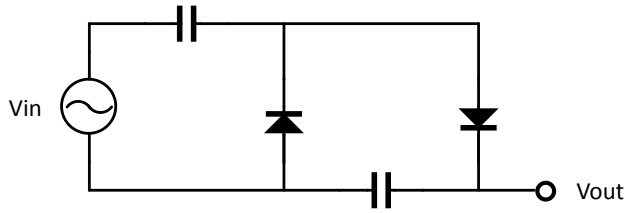

Fig.2. Unit cell of the CW circuit.

Figure 3 shows the circuit model of the *LCR* series circuit. The output voltage is obtained from both sides of L_S or C_S with a high impedance load. The absolute value of the current I_S ($|I_S|$) in this circuit is given by

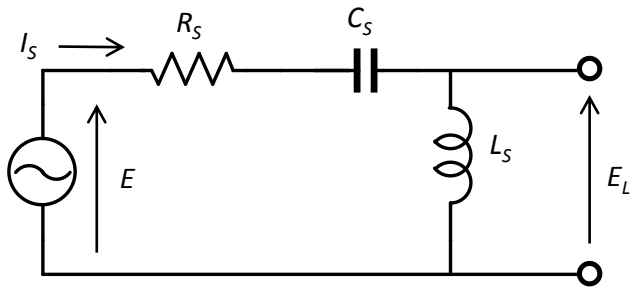

Fig. 3. Circuit model of the *LCR* series circuit.

Figure 4 shows the circuit model of the proposed booster circuit [19]. In Fig. 4, the input impedance is set to 50 Ω. To enhance the RF voltage amplitude, L (= 15 nH) and C_C (= 0.3 pF) are used in the main resonant circuit. C_1 (= 0.3 pF) is the tuning block for compensating the tolerance of the discrete components and obtaining a high voltage swing at the centre frequency. Here, C_2 (= 0.3 pF) is an impedance matching capacitor. The two-stage CW circuit is composed of a diode (HSMS-286Y, Avago), C_2 and C_3 (= 15 pF). In the input section, an AC voltage source and a 50-Ω internal resistance (R) are connected in place of the antenna. The DC output of the proposed circuit is numerically analysed using the ADS (Keysight technologies) circuit simulator.

Figure 5 shows the typical simulation results of the relationship between V_{out} / V_{LC} and N, where V_{LC} represents the output voltage of the resonant circuit—namely, the input of the CW circuit. From Fig. 5, Eq. (1) is not satisfied because of the

parasitic elements of the diodes, and there is an optimized number for the unit structure in the RF region. The input impedance of the booster circuit is changed slightly by increasing *N*; hence, the capacitance values are optimized as mentioned in the previous paragraph.

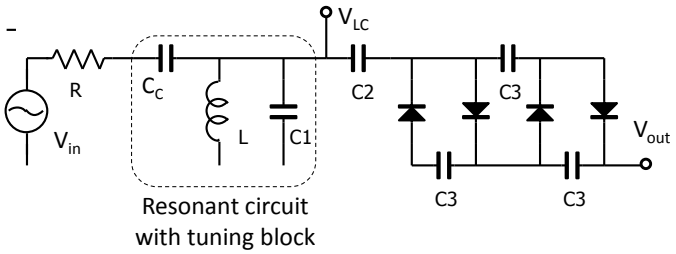

Fig.4. Circuit of the proposed booster circuit.

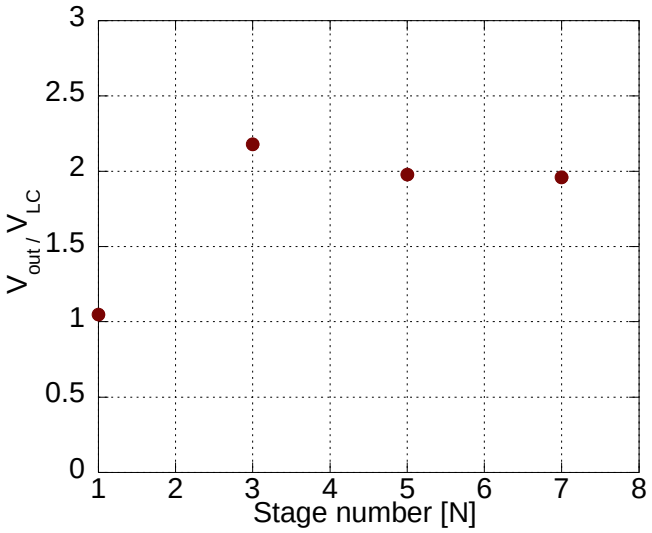

Fig. 5. Simulation results of the relationship between V_{out} / V_{LC} and *N*.

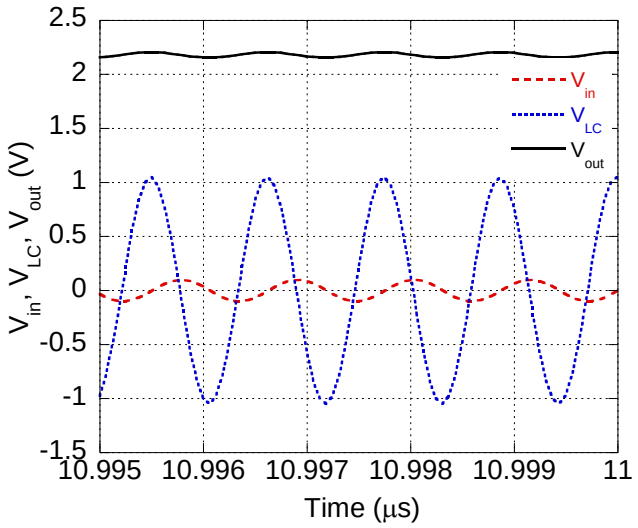

Fig. 6. Transient analysis of V_{in}, V_{LC} and V_{out} at 900 MHz.

Figure 6 shows the simulated voltage of the source (V_{in}), V_{LC}, and V_{out} in the booster circuit. Here, V_{in} is 100 mV at 900 MHz, and V_{LC} is set to be 10 times greater than V_{in} by passing it through the resonant circuit. Because the RF signal is boosted and rectified by the CW circuit, V_{out} is 23 times greater than V_{in}, and the proposed energy harvesting circuit generates an approximately time-independent output voltage.

The RF-to-DC power conversion efficiency (η) is defined as follows [20]:

$$\eta = \frac{DC\ output\ \ power}{RF\ \ input\ \ power} \qquad (7)$$

Figure 7 shows the simulated power conversion efficiency dependency on the load resistance (R_L), where the RF input power is –10 dBm. The maximum η in this study is 57.8% for R_L=1.0 × 10^7 Ω.

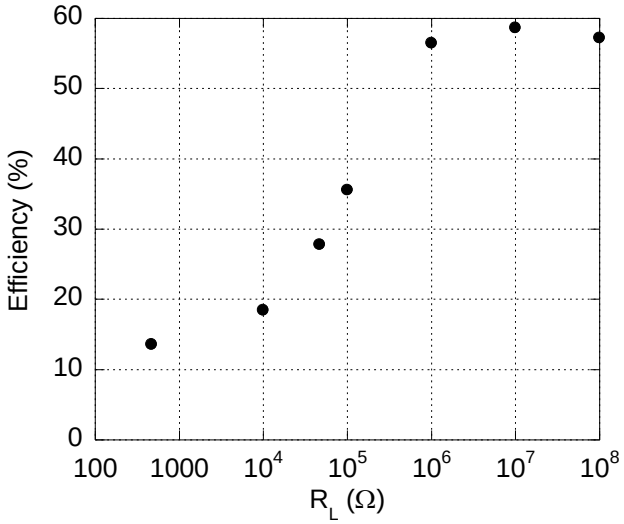

Fig. 7. Power conversion efficiency dependency on load resistance (R_L) at 900 MHz

III. Impedance Matching Circuit Design

Our proposed energy harvesting circuit is placed on the backside of a one-sided directional planar antenna fabricated on a flexible substrate. A slot dipole antenna was chosen for our system. To miniaturize the slot size of the antenna, an impedance matching circuit is necessary. This antenna is called an electrically small antenna (ESA). The impedance matching circuit in the ESA that we propose is composed of a CPW transmission line and interdigital gap, and the design method is the same as was proposed previously [13].

Our proposed impedance matching circuit is based on a Chebyshev bandpass filter (BPF) [22, 23]. The BPF is composed of a resonance circuit and impedance inverter (K-inverter, $K_{i,\,i+1}$). A one-stage BPF is used to reduce the circuit size.

Figure 8 shows the one-stage BPF composed of K-inverters given by

$$K_{0,1} = \sqrt{w}\sqrt{\frac{Z_0 x_1}{g_0 g_1}}, \quad K_{1,2} = \sqrt{w}\sqrt{\frac{x_1 Z_0}{g_1 g_2}} \tag{8}$$

$$X_1 = x_1\left(\frac{\omega}{\omega_0} - \frac{\omega_0}{\omega}\right) \tag{9}$$

where X_1 is the reactance of the transmission line, which has a reactance slope parameter x_1. w is a relative bandwidth, and g_i is the filter parameter. ω and ω_0 are the angular velocity and the resonance angular velocity, respectively.

At the centre frequency, the equivalent circuit model is described as shown in Fig. 9. In this case, the resonance condition is given by

$$R'_L = \frac{K_{0,1}^2}{Z_0} = \frac{w x_1}{g_0 g_1} \tag{10}$$

$$R'_S = \frac{K_{1,2}^2}{Z_0} = \frac{w x_1}{g_1 g_2} \tag{11}$$

A quality factor of this resonance circuit (Q) is obtained by

$$Q = \frac{x_1}{R'_S + R'_L} = \frac{g_0 g_1 g_2}{w\left(g_0 + g_2\right)} \tag{12}$$

Substituting Eq. (10) for Eq. (11), the resistance ratio is given by

$$\frac{R'_L}{R'_S} = \frac{g_0}{g_2} \ . \tag{13}$$

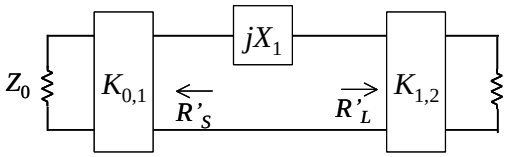

Fig. 8. Circuit model of the one-stage BPF with a K-inverter.

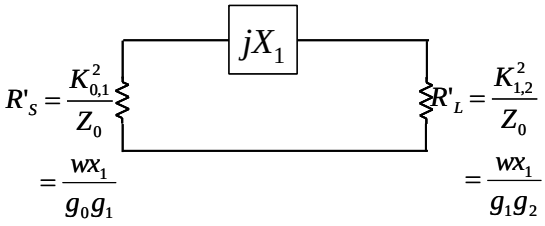

Fig. 9. Equivalent circuit of the circuit shown in Fig. 8 at the resonance frequency.

Next, the design of the miniaturized impedance matching circuit using a quarter-wavelength (λ/4) transmission line was presented.

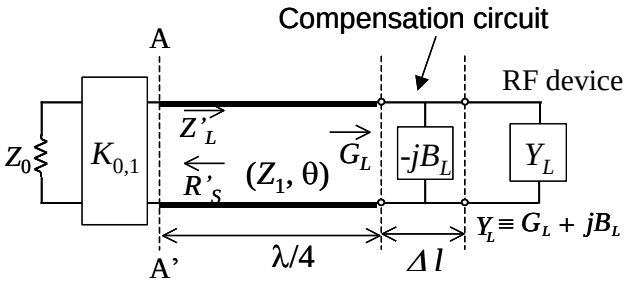

Fig. 10. Circuit model of the proposed impedance matching circuit.

Figure 10 shows the circuit model of the proposed transmission-line-based impedance matching circuit. Generally, an RF device has an admittance Y_L of

$$Y_L = \frac{1}{Z_L} \equiv G_L + jB_L \tag{14}$$

To compensate B_L, the length of the transmission line is optimized by

$$\Delta l = -\frac{B_L}{\omega_0 C} \tag{15}$$

where C [F/m] is the capacitance per unit length in the transmission line.

In Fig. 10, Z_L' and R_S' are described as

$$Z'_L = Z_1^2 G_L + jX_1 \equiv R'_L + jX'_L \tag{16}$$

$$X_1 = -Z_1 \cot\theta \equiv x_1\left(\frac{\omega}{\omega_0} - \frac{\omega_0}{\omega}\right) \tag{17}$$

$$x_1 = \frac{\pi}{4} Z_1 \tag{18}$$

$$R'_S = \frac{K_{0,1}^2}{Z_0} \tag{19}$$

where Z_1 and θ are the characteristic impedance and electrical length of the transmission line, respectively. The admittance (Y_L) of the RF device is assumed to be $|Y_L| << Y_0$. At the resonance frequency, X_1 in Eq. (17) goes to zero. In this case, the equivalent circuit model at A-A' in Fig. 10 can be modified as shown in Fig. 11.

Considering the resonance condition of Eqs. (12) and (13),

we can obtain the resistance ratio and Q value at the resonance frequency as follows.

$$\frac{R'_L}{R'_S} = \frac{Z_0}{K_{0,1}^2} Z_1^2 G_L = \frac{g_0}{g_2} \tag{20}$$

$$Q = \frac{x_1}{R'_S + R'_L} = \frac{Z_0}{K_{0,1}^2} \frac{x_1}{\left(1 + \frac{g_0}{g_2}\right)} = \frac{g_0 g_1 g_2}{w(g_0 + g_2)} \tag{21}$$

By solving Eqs. (20) and (21), the final design equations are given by

$$Z_1 = \frac{\pi}{4} \frac{w}{g_1 g_2 G_L} \tag{22}$$

$$K_{0,1} = \sqrt{w} \sqrt{\frac{Z_0 x_1}{g_0 g_1}}, \quad \left(x_1 = \frac{\pi}{4} Z_1\right) \tag{23}$$

The input impedance is matched by using the λ/4 transmission line, which has a characteristic impedance (Z_1) and K-inverter ($K_{0,1}$).

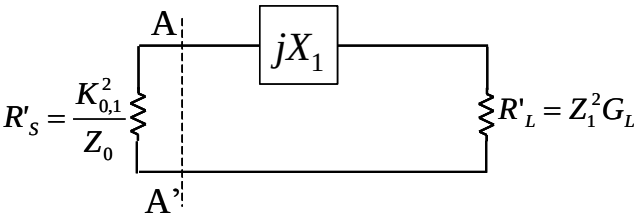

Fig. 11. Equivalent circuit model of the circuit shown in Fig. 10 at the resonance frequency.

IV. Antenna Design

Our proposed impedance matching circuit is implemented in an antenna. Figure 12 shows the layout of the one-sided directional slot antenna on the flexible substrate (Duroid RT6010, Rogers). The designed centre frequency is the 900 MHz band. The cross-sectional view of this antenna is also shown in Fig. 12. To suppress the backward radiation, the floating metal layer is attached to the bottom of the substrate. The substrate has dielectric constant ε_r=10.2 and tanδ = 0.0023. The thickness of the substrate and both copper metals are 1.27 mm and 18 μm, respectively. Figure 13 shows a close-up of the interdigital gap. To realize the 50-Ω impedance matching, the number of teeth, tooth length, and tooth width are optimized.

The simulated electric field distribution of a top metal and a bottom floating metal layer are shown in Fig. 14. The top layer resonates; however, the bottom floating metal layer does not resonate. Thus, this floating metal layer can suppress the radiation of the backward radiation (bottom side), and the directivity of the forward direction is greater than that of the backward direction.

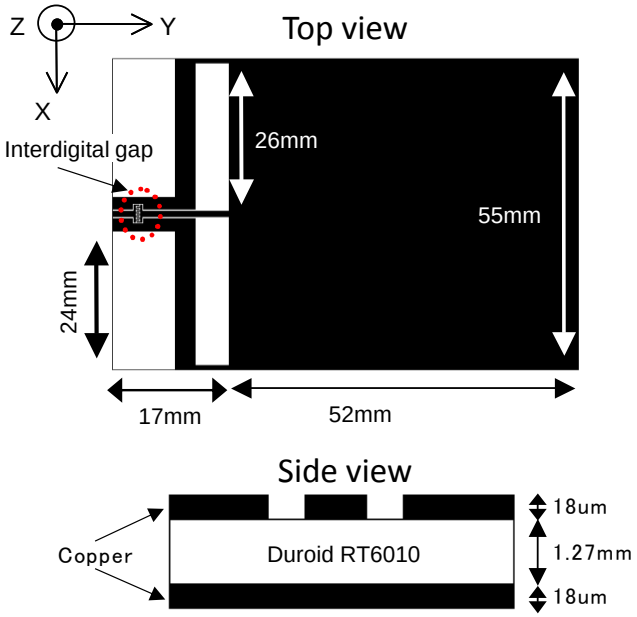

Fig. 12. Layout of the one-sided directional slot antenna on the flexible substrate.

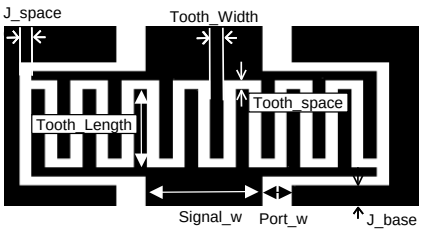

Name	Size [mm]
J_space	0.12
J_base	0.12
Tooth_length	0.95
Tooth_width	0.12
Tooth_space	0.12
Signal_w	1.00
Port_w	0.26

Fig. 13. Close-up of the interdigital gap.

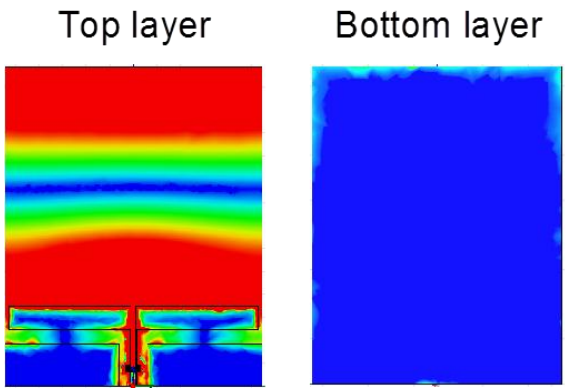

Fig. 14. Electric field distribution of a top metal and a bottom floating metal layer.

Figure 15 shows the input impedance (Z_{in}) of this antenna. At 900 MHz, Z_{in} is 47.94 – j 0.65 Ω, which is almost the same as 50 + j 0 Ω. Thus, the impedance matching circuit is deemed operational.

Because this substrate is flexible, the return loss and radiation characteristics of this antenna were simulated as if this antenna were bent. Figure 16 shows the cross-sectional view for the simulation condition. In the figure, θ is the bending angle. Figures 17 and 18 show the frequency responses and radiation patterns of our proposed antenna with different values of θ. The matching frequency (centre frequency), matching bandwidth, and radiation patterns are almost the same over the different θ values. This antenna maintains the one-sided directional radiation if it is bent.

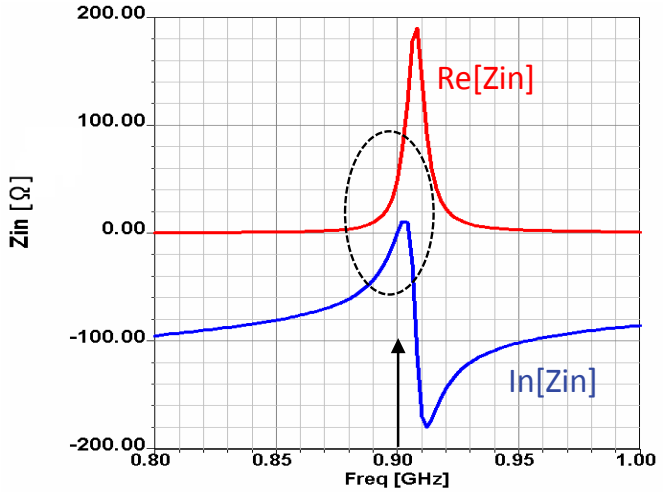

Fig. 15. Simulated input impedance of the proposed antenna.

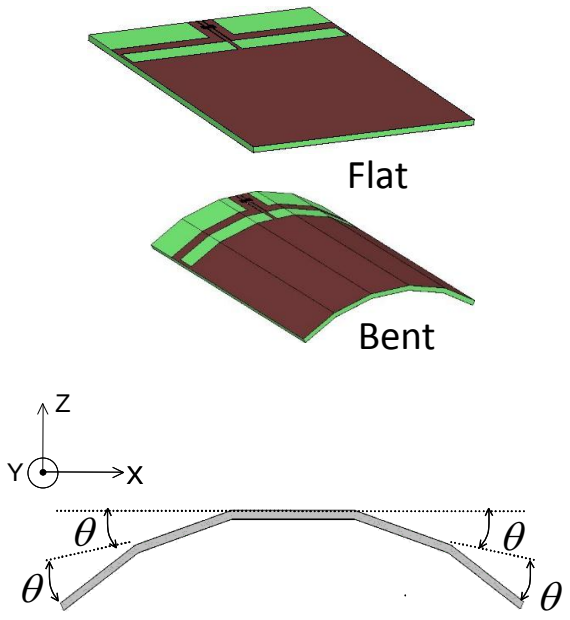

Fig. 16. Simulation condition of the bending angle.

V. Measurement Results of the Circuit

Figure 19 shows a photograph of the booster circuit, which has an input impedance = 50 Ω. All capacitors, inductors, and diodes are placed on the top metal of the microstrip transmission line and are connected by solder. The dimensions of the booster circuit are 2.0 mm × 1.6 mm. The ground metal plane is placed on the backside of this circuit. Figure 20 shows the frequency dependence of the output voltage of the proposed energy harvesting circuit. In the figure, the solid line shows V_{out} calculated from Fig. 4—namely, without parasitic components—where the RF input is 100 mV. The dotted line shows the measured results. Compared with the ideal values, the measured centre frequency and peak voltage are lower, and the bandwidth is wider. The measured power efficiency is 44%. Because of the parasitic components due to the resistance of electrical contacts to the printed circuit board (PCB), the characteristic impedance of the transmission line on the PCB, inductance of the RF feed lines, and tolerance of the chip components, the centre frequency and quality factor of the circuit are reduced. The tolerances of the capacitor and inductor are 0.1 pF and 5%, respectively. The characteristic impedance and metal loss of the microstrip transmission lines, which have a 1 mm line width, are also considered. The broken line shows the simulation results with the above parasitic components. The measured results are good agreement with the simulation results of parasitic components.

Table I summarizes the performance of the proposed circuit compared with the recently published work. The efficiency is higher than those in previous research. In each case, the input power is similar to and lower than a similar wireless power transfer system, and the efficiency is less than 50%. From the results of our proposed circuit, the series resonance circuit and impedance mating circuit in front of the CW circuit are strong tools for enhancing a weak RF input signal such as that in a wireless telecommunication system.

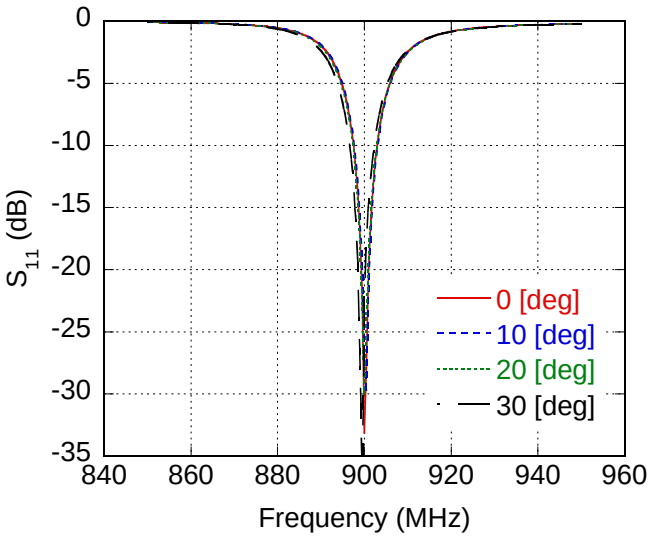

Fig. 17. Frequency responses of the slot antenna with different bending angles.

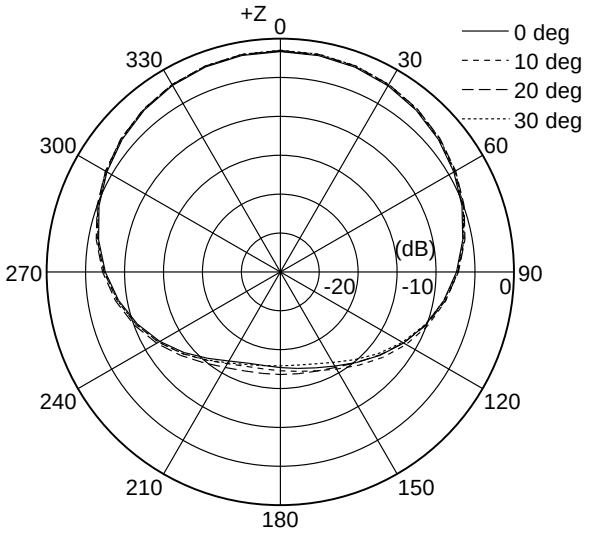

Fig. 18. Simulated radiation patterns of the slot antenna with different bending angles.

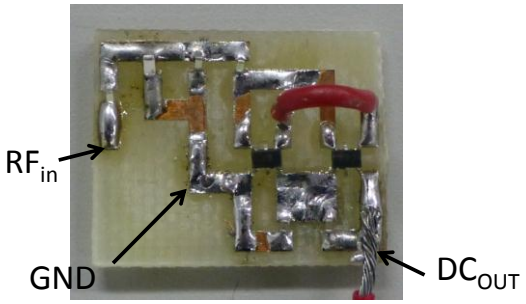

Fig. 19. Photograph of the proposed booster circuit.

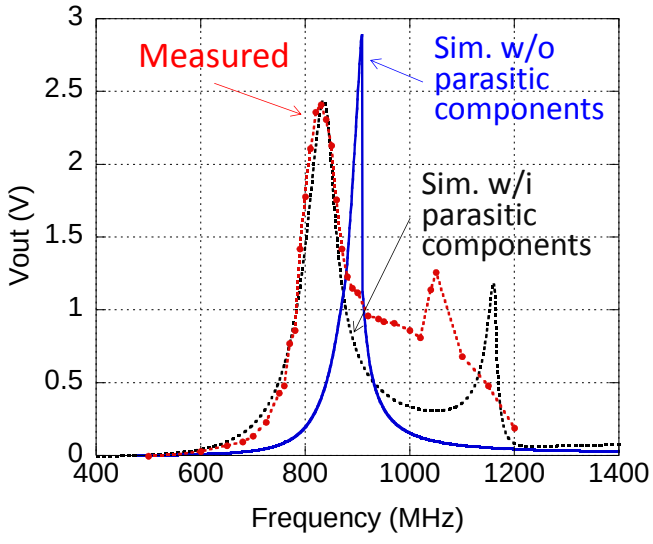

Fig. 20. Frequency responses of the output voltage of the proposed energy harvesting circuit.

Table.1. Comparison of the measured efficiency of the energy harvesting circuit for the UHF band

Ref.	Freq.(MHz)	Pin (dBm)	Efficiency (%)
[2]	850	-10	35
[3]	550	-10	45
[5]	896	-19	18
This work	830 900*	-10	44 58.7*

* Simulation w/o parasitic components.

VI. Measurement Results of the Antenna

Our proposed antenna was fabricated by using CAD-controlled milling machine. Figure 21(a) shows a photograph of this machine. Figure 21(b) shows a close-up of the drill section. There is a ϕ = 0.1 mm drill in this system. Figure 22 shows the photograph of the proposed antenna. The top metal layer (a) and bottom floating metal layer (b) are shown. The bottom floating metal layer is not connected. A close-up of the interdigital gap composed of impedance matching circuit (c) is also shown. The MMCX connector is attached at the input port.

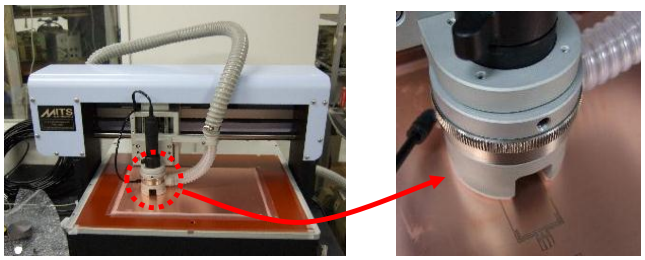

(a) Milling machine (b) Close-up of the drill

Fig. 21. Photograph of the proposed antenna.

The radiation patterns of this antenna are measured in the anechoic chamber. Figure 23 shows the layout of this chamber. Our proposed antenna was placed on the turntable on the left, and the angular dependence of the receiving signal was measured by rotating the turntable. Figure 24 shows a photograph of the chamber. A wideband horn antenna (up to 18 GHz) was used as a reference transmitting antenna. The distance between the reference antenna and our proposed antenna is 2.5 m.

Figure 25 shows a photograph of the flat antenna and the antenna after being bent. This antenna is flexible; hence, it is easy to revert to the original flat structure. Figure 26 shows a comparison of the return loss with different values of θ. These data are similar and agree with the simulation results in Fig. 17. However, the centre frequency is slightly shifted to a lower region because of the error in the dielectric constant of the substrate. Figure 27 shows the measured radiation patterns at 900 MHz, where "Flat" represents θ = 0 degree and "Bend" represents θ = 17 degrees, respectively. The measured front-to-back ratio (F/B ratio) is approximately 10 dB. As shown in Fig. 27, our proposed antenna maintains the one-sided

directional radiation if θ increases. Thus, we can realize the one-sided directional antenna on a flexible substrate. This antenna can work if it is mounted on nonplanar objects. The booster circuit can be connected to the backside of this antenna.

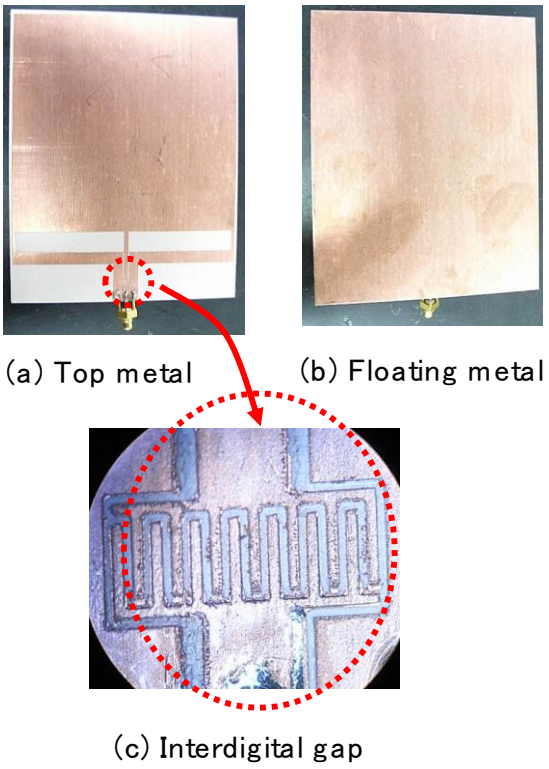

Fig. 22. Photograph of the proposed antenna.

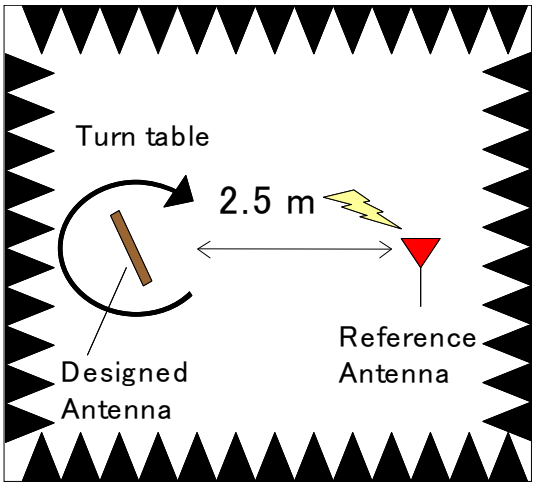

Fig. 23 Layout of the measuring setup.

We also attempted to light an LED without connecting it to a power source by wires.

The 900 MHz band is one of the ISM (industry, science, medical) bands that are operated without licenses. UHF RFID tag systems operating at the 900 MHz band are used worldwide. The output power of the UHF RFID transmitter is 250 mW, which is suitable for the RF energy harvesting system, because it is higher than the Wi-Fi transmitter power.

Figure 28 shows a photograph of the LED light-up demonstration with the energy harvesting circuit on the backside of the antenna. The antenna gain of both the transmitting and receiving antennas is -0.7 dBi. The distance between antennas is 0.2 m. The transmission signal power at the output port of a signal generator is 20 dBm. As can be seen, the LED is operational. Because the V_f (forward voltage) of this LED is 2.0 V, our proposed energy harvesting system generates at least 2 VDC of voltage, confirming the data in Fig. 6.

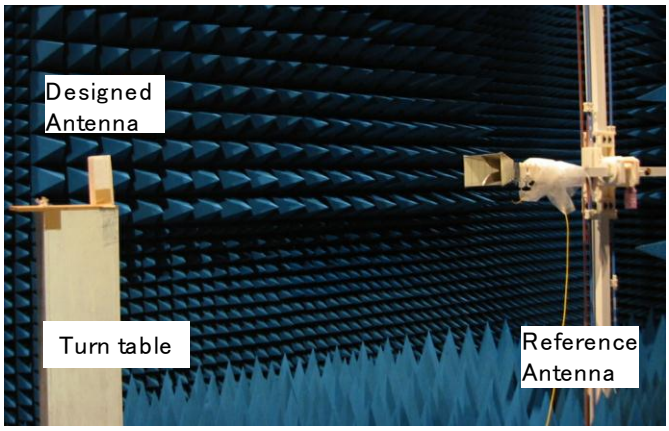

Fig. 24 Photograph in the anechoic chamber.

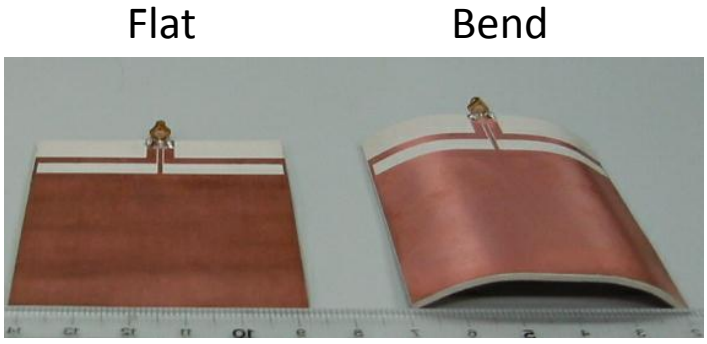

Fig. 25. Photograph of the flat antenna and the antenna after being bent.

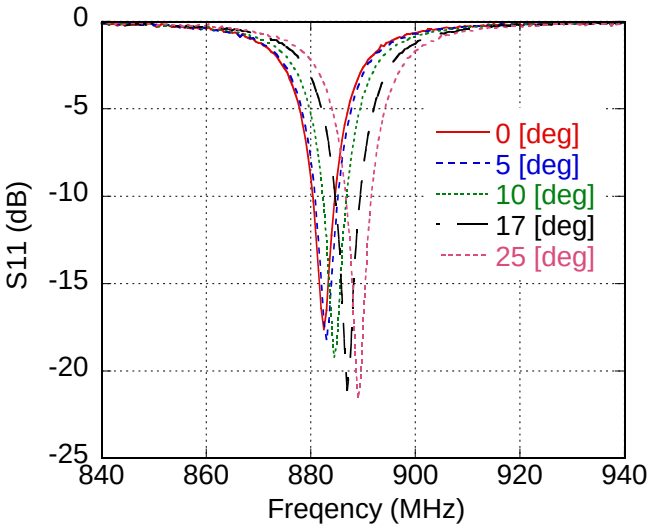

Fig. 26. Comparison of the return loss with different θ values (measured).

VII. Conclusions

This paper describes the design of an RF-to-DC energy harvesting circuit. The circuit was composed of a one-sided directional antenna on a flexible substrate, an impedance matching circuit, a resonant circuit, and a booster circuit for converting and boosting radio frequency power into DC voltage. A transmission-line-based impedance matching circuit was implemented on the one-sided directional slot antenna. This antenna is composed of a top metal layer and a bottom floating metal layer. The measured F/B ratio is approximately 10 dB, and the antenna gain is –0.7 dBi. The simulated conversion efficiency of the proposed boosting circuit without any parasitic elements is 58.7%. Owing to the effect of the parasitic components in the circuit, the measured efficiency was 44%. By using the backside of the proposed antenna on the flexible substrate, the DC voltage is directly generated, and the LED is operated.

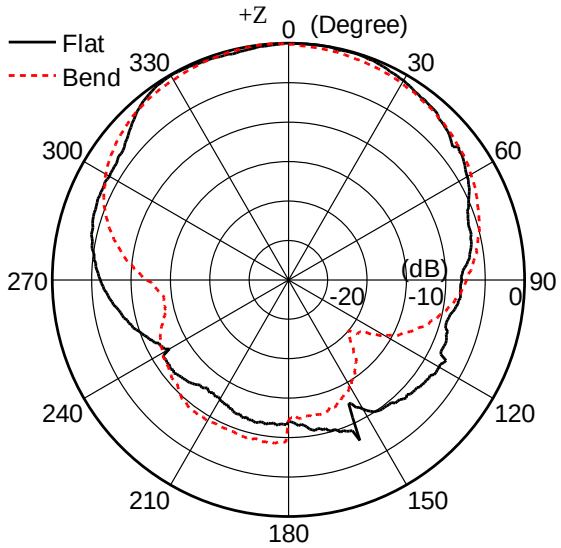

Fig. 27. Measured radiation patterns at 900 MHz. (θ = 0 deg (Flat) and θ = 17 deg, (bend))

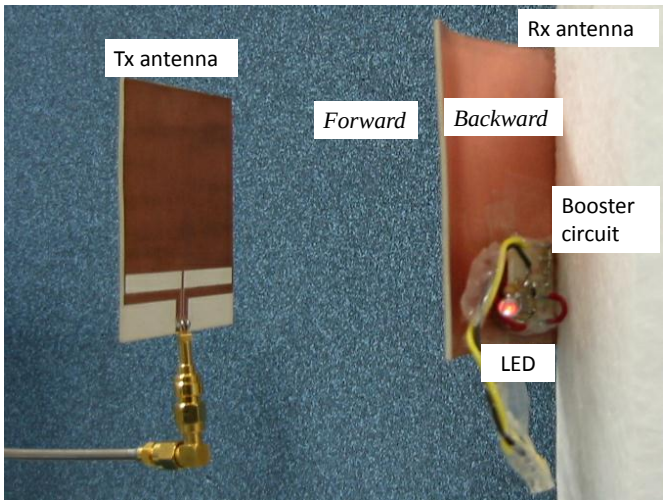

Fig. 28. Photograph of the LED light-up demonstration for the power harvesting circuit on the antenna.

Acknowledgements

This work was partly supported by the VLSI Design and Education Center (VDEC), the University of Tokyo in collaboration with CADENCE Corporation and Keysight Corporation. This work was partially supported by the Grant-in-Aid for Scientific Research (KAKENHI) from Japan Society for the Promotion of Science, JSPS. This research was also partially supported by the Grant-in-Aid for Collaborative Research Program Based on Industrial Demand, CREST and Matching planner program from Japan Science and Technology Agency, JST.

The author would like to express thanks to Miss Yuharu Shinki and Mr. Kyohei Shibata in Kyusshu University, Japan and Mr. Mohamed Mansour at the Electronics Research Institute, Dokki, Egypt, for their help and support.

References

[1] A. Shameli, A. Safarian, A. Rofougaran, M. Rofougaran, and F. D. Flaviis, "Power harvester design for passive UHF RFID tag using a voltage boosting technique", *IEEE Trans. Microwave. Theory Tech.*, vol. 55, no. 6, pp. 1089–1097, June 2007.

[2] A. Georgiadis, A. Collado, S. Via, and C. Meneses, "Flexible hybrid solar/EM energy harvester for autonomous sensors", *IEEE IMS 2011 Digest*, pp. 1–4, June 2011.

[3] C. Mikeka and H. Arai, "Microwave tooth for sensor power supply in battery-free applications", Proc. Asia Pacific Microw. Conf., pp. 1802–1805, Dec 2011.

[4] A. Sample, and J. R. Smith1, "Experimental results with two wireless power transfer systems", *Proc. IEEE Radio and Wireless Symposium*, pp. 16–18, Jan. 2009.

[5] U. Karthaus and M. Fischer, "Fully integrated passive UHF RFID transponder IC with 16.7-uW minimum RF input power", *IEEE J Solid-State Circuits*, vol. 38, no. 10, pp. 1602–1608, Oct. 2003.

[6] J. P. Curty, N. Joehl, F. Krummenacher, C. Dehollain, and M. J. Declercq, "A model for u-power rectifier analysis and design", *IEEE Trans Circuit Systems*, vol. 52, no. 12, pp. 2771–2779, Dec. 2005.

[7] H. Kitayoshi and K. Sawaya, "Long range passive RFID-tag for sensor networks", *Proc. IEEE Vehicular Tech. Conf.*, pp. 2696–2700, Sept. 2005.

[8] Cockcroft-Walton generator, http://en.wikipedia.org/wiki/Cockcroft Walton generator

[9] C. Cho, H. Choo, and I. Park, "Design of planar RFID tag antenna for metallic objects", *Electron. Lett.*, vol. 44, pp. 175–177, 2008.

[10] Q. Z. Chen and B. J. Hu, "Novel UHF RFID tag antenna with shorted stubs mountable on the metal objects", *Microwave and Millimeter Wave Technology*., pp 1822–1824, 2008.

[11] D. D. Arumugam, and D. W. Engels, "Characteristics of passive UHF RFID tags on metalslabs", *Proc. IEEE Antennas and Propagation Society International Symposium*, pp.1–4, June, 2009.

[12] T. W. Koo, D. Kim, J. I. Ryu, J. K. Kim, J. G. Yook, and J. C. Kim, “Design and Implementation of Label-type UHF RFID Tags for the Metallic Object Application”, *Proc. IEEE Antennas and Propagation Society International Symposium*, 206.6, June, 2010.

[13] H. Kanaya, R. Nabeshima, R. K. Pokharel, K. Yoshida, M. Tsujii, and R. Iino, “Development of an Electrically Small One-Sided Directional Antenna with Matching Circuit”, *Proc. 2008 IEEE Radio and Wireless Symposium*, pp. 739–742, 2008

[14] H. Urabe, R. K. Pokharel, H. Kanaya, K. Yoshida, A. Ishikawa, S. Fukagawa, and A. Tahira, “Design and Performance of 800MHz/2GHz Dual Band Small Planar Antenna”, *Asia-Pacific Microwave Conference Proceedings*, pp. 1508, Dec. 2009.

[15] H. Kanaya, M. Kato, R. K. Pokharel, and K. Yoshida, “Development of 2.4GHz One-Sided Directional Planar Antenna with Quarter Wavelength Top Metal”, *Proc. 2010 IEEE International Symposium on Antennas & Propagation*, 404.1, 2010.

[16] H. Kanaya, J. Fujiyama, G. Urakawa, and K. Yoshida, "Design and Performance of High Tc Superconducting Coplanar Waveguide Matching Circuit for RF-CMOS LNA", *IEICE transactions on electronics*, vol. 86, no. 1, pp. 37–42, 2003.

[17] H. Kanaya, T. Shinto, K. Yoshida, T. Uchiyama, and Z. Wang, "HTS coplanar waveguide bandpass filters with highly packed meanderlines", *IEEE Trans Appl. Supercond*., 11, pp. 481–484, 2001.

[18] T. Hirabaru, H. Kanaya, D. Kanemoto, R. K. Pokharel, K. Yoshitomi, and K. Yoshida, "Development of 900MHz band one-sided directional antenna on flexible substrate", *Proc. IEEE Antennas and Propagation Society International Symposium*, pp. 1008–1011, July 2011.

[19] H. Kanaya, S. Tsukamoto, T. Hirabaru, D. Kanemoto, R. K. Pokharel, and K. Yoshida, "Energy Harvesting Circuit on a One-Sided Directional Flexible Antenna", *IEEE Microwave and Wireless Components Letters*, vol. 23, no. 3, pp. 164–166, 2013.

[20] V. Mariani and M. Thevenot, "Efficient design of rectifying antennas for low power detection", *IEEE IMS 2011 Digest*, pp. 1–4, June 2011.

[21] H. Kanaya, Y. Koga, G. Urakawa, and K. Yoshida, “Design of HTS Coplanar Waveguide Matching Circuit for Low Noise CMOS-HTS Receiver”, *IEEE Trans Appl. Supercond.*, vol. 13, pp. 1031–1034, 2003.

[22] G. Matthaei, L. Young, and E. Jones, “Microwave Filters, Impedance-Matching Networks, and Coupling Structures”, New York: *McGraw-Hill*, 1964, pp. 427–440.

[23] H. Kanaya, J. Fujiyama, R. Oba, and K. Yoshida, “Design method of miniaturized HTS coplanar waveguide bandpass filters using cross coupling”, *IEEE Trans Appl. Supercond*., vol. 13, pp. 265-268, 2003.